Genetically targeted magnetic control of the nervous system

Michael A Wheeler[1,2], Cody J Smith[1,7], Matteo Ottolini[3,7], Bryan S Barker[2,3], Aarti M Purohit[1], Ryan M Grippo[1], Ronald P Gaykema[3], Anthony J Spano[1], Mark P Beenhakker[4], Sarah Kucenas[1,5], Manoj K Patel[3], Christopher D Deppmann[1,5,6] & Ali D Güler[1]

Optogenetic and chemogenetic actuators are critical for deconstructing the neural correlates of behavior. However, these tools have several limitations, including invasive modes of stimulation or slow on/off kinetics. We have overcome these disadvantages by synthesizing a single-component, magnetically sensitive actuator, "Magneto," comprising the cation channel TRPV4 fused to the paramagnetic protein ferritin. We validated noninvasive magnetic control over neuronal activity by demonstrating remote stimulation of cells using *in vitro* calcium imaging assays, electrophysiological recordings in brain slices, *in vivo* electrophysiological recordings in the brains of freely moving mice, and behavioral outputs in zebrafish and mice. As proof of concept, we used Magneto to delineate a causal role of striatal dopamine receptor 1 neurons in mediating reward behavior in mice. Together our results present Magneto as an actuator capable of remotely controlling circuits associated with complex animal behaviors.

Opto- and chemogenetic actuators have revealed critical properties of neural networks in normal and pathological states[1–6]. While both opto- and chemogenetics remotely control neuronal stimulation, optical strategies are limited spatially by poor light penetration into dense tissues and chemogenetic strategies suffer from slow pharmacokinetics that prevent cellular activation on a physiologically relevant timescale. Therefore, there remains a need for next-generation actuators that are noninvasive and can respond rapidly and reversibly[7]. Several recent studies have reported transient receptor potential vanilloid 1 (TRPV1) ion channels can be engineered to become sensitive to a combination of radio waves and magnetothermal heating through coupling to the iron storage protein ferritin or to inorganic paramagnetic nanoparticles[8–12]. While these reagents represent an important advance, they are multicomponent systems (requiring, for example, delivery of nanoparticles and a genetically encoded channel) with possible off-target heating effects. One study employed nonthermal magnetogenetic control of somatic tissues to regulate blood glucose[11], but a genetically encoded, single-component magnetogenetic system has yet to be applied to the nervous system. Here we have expanded

on these strategies by engineering a magnetogenetic actuator through fusion of the nonselective cation channel TRPV4 (refs. 13–15) to the paramagnetic protein ferritin[16]. We have successfully applied this actuator to the nervous system and validated it using *in vitro* calcium imaging, brain slice electrophysiology, *in vivo* electrophysiology and acute modulation of behavior in freely moving zebrafish and mice.

RESULTS

Design and screen of a magnetically sensitive cation channel

To engineer a single-component magnetogenetic actuator, we based our design on TRPV4 because it has been reported to respond to pressure[13,14]. We suspected that, when fused to TRPV4, a paramagnetic protein would enable magnetic torque to tug open the channel to depolarize cells (**Supplementary Fig. 1**). While we hypothesized that magnetic force–dependent activation of TRPV4 would be easier than in the case of a non-mechanically sensitive ion channel, it is also formally possible that application of torque to ion channels in general would achieve the same result. Therefore, we developed a small library of 21 proteins consisting of TRPV4 (rat *Trpv4*) fused to a gene encoding two subunits of the paramagnetic ferritin protein (human *FTL* and *FTH1*) (**Supplementary Table 1**)[17]. Human embryonic kidney (HEK) 293 cells did not express 18 of the 21 generated chimeric proteins following transient transfection, presumably because of cytotoxicity of the chimeric channels. For the three channels that did express in HEK293 cells, we performed *in vitro* calcium imaging to determine whether the fusion proteins responded to magnetic fields. Using the fluorescent calcium-binding dye Fluo-4, we measured calcium transients in response to a ~50-mT magnetic field delivered by an electromagnet (**Supplementary Fig. 2**). Of the three candidate proteins, we observed detectable calcium transients in response to magnetic stimulation with one fusion protein, consisting of ferritin tethered to a truncated TRPV4 carboxy terminus (Δ760–871) (**Supplementary Fig. 3**).

Because the 17 ± 3.5% (mean ± s.e.m.) increase in magnetically evoked calcium transients was smaller than expected TRPV4 responses[15] (**Supplementary Fig. 3h**), we hypothesized that trafficking to the plasma membrane was disrupted[18], resulting in blunted calcium signaling. We next optimized the chimeric channel's subcellular

[1]Department of Biology, University of Virginia, Charlottesville, Virginia, USA. [2]Neuroscience Graduate Program, University of Virginia, Charlottesville, Virginia, USA. [3]Department of Anesthesiology, University of Virginia, Charlottesville, Virginia, USA. [4]Department of Pharmacology, University of Virginia, Charlottesville, Virginia, USA. [5]Department of Cell Biology, University of Virginia, Charlottesville, Virginia, USA. [6]Department of Biomedical Engineering, University of Virginia, Charlottesville, Virginia, USA. [7]These authors contributed equally to this work. Correspondence should be addressed to A.D.G. (aguler@virginia.edu).

Figure 1 Remote control of calcium signaling using Magneto2.0.
(**a**–**e**) *In vitro* calcium imaging micrographs of Fluo-4-loaded HEK293
cells before and after three pulses of 40–50 mT, 0.1 Hz, 90% duty cycle
magnetic stimulation. (**f**) Quantification of calcium fluorescence fold
change in response to the given condition. All experiments treated with
magnetic fields except "no magnet" condition. Replicates are shown as
individual coverslips; coverslips per condition: $n = 5$ (TRPV4 and ferritin),
$n = 3$ (no magnet), $n = 4$ (ruthenium red (RR)), $n = 4$ (Ca^{2+} free),
$n = 5$ (magnet); total cells analyzed per condition are $n = 195$ (TRPV4
and ferritin), $n = 150$ (no magnet), $n = 148$ (RR), $n = 206$ (Ca^{2+} free),
$n = 396$ (magnet) with $n > 30$ cells analyzed per coverslip. One-way
ANOVA, Bonferroni post-test ($F_{4,16} = 7.268$, $P = 0.0016$). (**g**) Average
kinetics of all cells analyzed on a single coverslip per condition ($n = 48$
(TRPV4 and ferritin), $n = 50$ (no magnet), $n = 45$ (RR), $n = 45$ (Ca^{2+} free),
$n = 102$ (magnet)). Horizontal bar with horseshoe indicates magnetic field
application. Two-way ANOVA, Bonferroni post-test ($F_{4,32490} = 199.1$,
$P < 0.0001$), $*P < 0.05$ for all time points from 250 s onward compared
to magnet condition. (**h**) Kinetics of calcium fluorescence fold change in
mCherry$^+$ cells in response to magnet in the presence or absence of
the TRPV4 inhibitor GSK205 (10 μM). $n = 3$ coverslips per condition.
Data represent all mCherry$^+$ cells analyzed ($n = 88$ GSK205-treated,
$n = 57$ untreated). Two-way ANOVA, Bonferroni post-test ($F_{39,5680} = 23.7$,
$P < 0.0001$), $***P < 0.0001$ for all time points from 30 s onward.
$***P < 0.001$, $**P < 0.01$, $*P < 0.05$. Data shown as mean ± s.e.m.
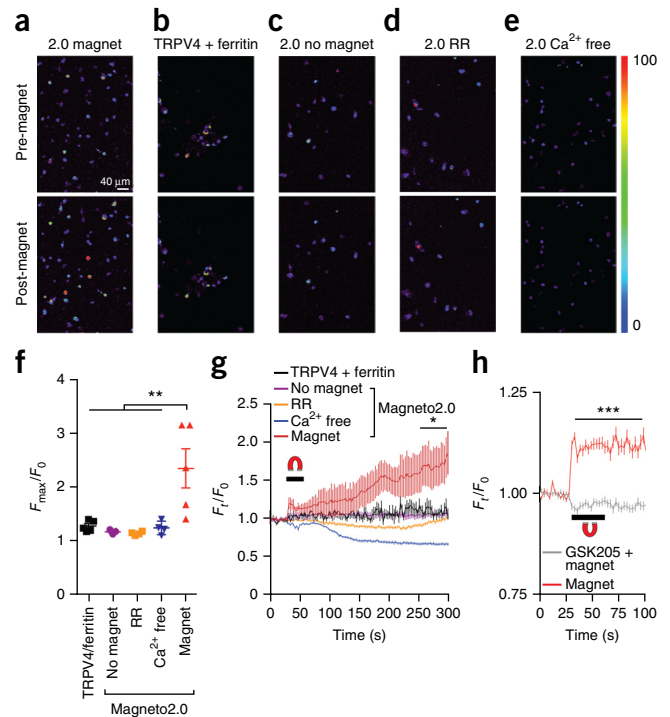
localization by adding a series of subcellular trafficking signals to
this protein, Magneto, as was done during the optimization of optoge-
netic actuators[19,20]. Ultimately, we determined that the addition of a
plasma membrane trafficking signal enhanced the prototype channel's
membrane expression (**Supplementary Fig. 4**), and we dubbed this
improved channel "Magneto2.0." We confirmed that HEK293 cells
were viable after Magneto2.0 expression (**Supplementary Fig. 5**) and
then measured magnetic field dependent calcium transients produced
by Magneto2.0 using the procedure described in **Supplementary
Figure 3**. Cells expressing Magneto2.0 (58% transfected cells, $n = 6$
coverslips, $n = 539$ cells) exhibited robust calcium transients approxi-
mately 2.5-fold higher than baseline after 50-mT magnetic stimulation,
with no change in any of the control conditions (**Fig. 1a**–**f**). Controls
included cells expressing unfused TRPV4 and ferritin moieties,
unstimulated Magneto2.0-expressing cells, Magneto2.0-expressing
cells exposed to the TRP pore blocker ruthenium red (RR), and
Magneto2.0-expressing cells in Ca^{2+}-free extracellular medium. We
observed calcium influx immediately following magnetic stimulation,
but the maximal calcium fluorescence occurred minutes after mag-
netic field stimulation of Magneto2.0-expressing cells, a time course
that was not observed in any of the above control conditions (**Fig. 1g**).
We found that the delayed calcium response in Magneto2.0$^+$ cells
was caused by calcium release from intracellular stores following
magnetically induced depolarization because this secondary response
was eliminated following depletion of intracellular calcium stores by
thapsigargin, a sarcoendoplasmic reticulum calcium transport ATPase
pump inhibitor[21] (**Supplementary Fig. 6**).

We next sought to determine whether the increase in calcium
signaling concomitant with magnetic field stimulation was GSK205
sensitive, which would suggest that the signal is TRPV4 dependent[22].
We thus stimulated and quantified the change in calcium fluorescence
of mCherry$^+$ *Magneto2.0-p2A-mCherry*-transfected cells during mag-
netic field application in both the presence and absence of the specific
TRPV4 inhibitor GSK205. We observed a magnetic field dependent
calcium increase in the GSK205-untreated Magneto2.0-expressing
cells that was greater than the response in stimulated GSK205-treated
cells (two-way ANOVA, $P < 0.0001$) (**Fig. 1h**). Moreover, 70 ± 5.1%
(mean ± s.e.m.) of Magneto2.0$^+$ cells responded to magnetic fields
($n = 3$ coverslips, $n = 58$ cells), with an average maximal change in

calcium fluorescence of 29 ± 9.8% (mean ± s.e.m.) during stimulation,
compared to only 6.5 ± 0.9% (mean ± s.e.m.) for the GSK205-treated
population ($n = 3$ coverslips per condition, $n = 88$ GSK205-treated
cells, $n = 57$ untreated cells, unpaired two-tailed t-test, $t_{143} = 2.819$,
$P = 0.0055$). All observed changes in calcium fluorescence were
noticeably improved over those of the poorly trafficked prototype
channel (**Supplementary Figs. 3** and **4a**). These data demonstrate that
Magneto2.0 is a magnetically sensitive, genetically encoded actuator
that can manipulate cellular activity *in vitro*.

Electrophysiological characterization in mammalian brain

These preliminary experiments prompted us to precisely deter-
mine the temporal kinetics of Magneto2.0 activation because the
future utility of Magneto2.0 is contingent on its rapid activation in
response to magnetic fields in live tissues. To this end, we generated an
adeno-associated virus (AAV) to express Magneto2.0 in mammalian
cells under control of the cytomegalovirus (CMV) promoter using
the double-floxed inverse open reading frame (DIO) approach
(*CMV::DIO-Magneto2.0*). This strategy enables permanent Cre-
dependent expression of a reversed *lox* site–flanked gene through Cre-
lox–mediated recombination (**Fig. 2a**)[23]. We bilaterally injected the
medial entorhinal cortices (mECs) of wild-type mice with an AAV1
containing *CMV::DIO-Magneto2.0* and an AAV9 carrying Cre recom-
binase fused to enhanced green fluorescent protein (EGFP) under
control of the calcium/calmodulin-dependent protein kinase II-α
promoter (*Camk2a::Cre-EGFP*), which will express Magneto2.0 in
excitatory neurons (**Fig. 2b**). To test whether Magneto2.0 could elicit
action potentials (APs) in neurons from brain slice preparations in
response to magnetic fields, we recorded from EGFP$^+$ neurons in the
mEC of wild-type mice doubly transduced with AAVs carrying *CMV::
DIO-Magneto2.0* and *Camk2a::Cre-EGFP* under whole-cell current
clamp conditions. Upon application of a ~50-mT static magnetic field
delivered by a NdFeB rare earth magnet, neurons in the mEC reliably
fired a series of APs akin to spiking behavior evoked by injection of
300 pA of depolarizing current (**Fig. 2c** and **Supplementary Fig. 7a**).

Figure 2 Electrophysiological characterization of Magneto2.0 in mouse brain slices. (**a**) Schematic of viral vector. ITR, inverted terminal repeats; *CMV*, cytomegalovirus promoter; P, *loxP* site; 2, *lox2272* site. (**b**) EGFP immunostaining of a wild-type mouse brain slice showing areas of viral transduction. Hippocampus/entorhinal cortex was doubly transduced with two AAV vectors: AAV1 carrying *CMV::DIO-Magneto2.0* and AAV9 carrying *Camk2a::Cre-EGFP*. DG, dentate gyrus; sub, subiculum; EC, entorhinal cortex. (**c**) Magnetically evoked spike train of a current-clamped mEC neuron transduced with *Camk2a::Cre-EGFP* and *CMV::DIO-Magneto2.0*. Neuron was stimulated with a 50-mT static magnetic field delivered by a permanent magnet. The graded bar represents the magnetic field experienced by neurons during the initiation and cessation of magnetic stimulation as the permanent magnet was brought toward the brain slice using a micromanipulator. Magnetically evoked APs were abolished by bath application of 10 µM GSK205. (**d**) Sample trace from an EGFP⁺ current-clamped mEC neuron transduced with *Camk2a::EGFP* and *CMV::DIO-Magneto2.0* and thus not expressing Magneto2.0. No action potentials are elicited in response to magnetic stimulation. (**e**) Quantification of the number of spikes compared between current injection (*n* = 14 neurons, *n* = 5 mice) and magnetic stimulation (*n* = 12 neurons, *n* = 5 mice) for EGFP⁺ cells expressing Magneto2.0. No magnetically induced APs are observed during bath application of GSK205 (*n* = 3 neurons, *n* = 3 mice) or when Magneto2.0 is not expressed (300 pA, *n* = 6 neurons; magnet, *n* = 3 neurons; *n* = 3 mice). All neurons examined are from a total of *n* = 8 mice. Left panel: one-way ANOVA, Bonferroni post-test ($F_{2,26}$ = 4.301, P = 0.0243). Right panel: unpaired two-tailed *t*-test, (t_7 = 13.23, P < 0.0001). ***P < 0.001, *P < 0.05; ns, not significant. Data shown as mean ± s.e.m.
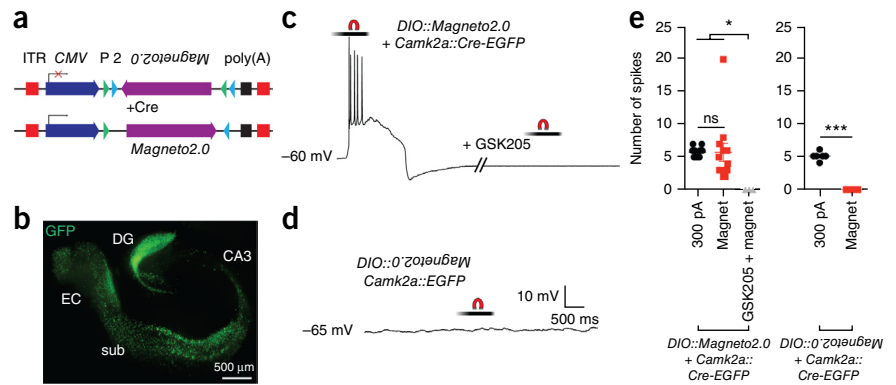
APs were elicited by both current injection and magnetic fields in 12 of 12 strongly EGFP⁺ neurons tested (*n* = 5 mice; *n* = 2 mice excluded due to low EGFP expression). Measurement of time to threshold and time to peak for APs evoked either by current injection or magnetic fields revealed no differences (**Supplementary Fig. 7b**). Membrane properties, such as resting membrane potential, AP amplitude, upstroke velocity, AP width and firing threshold were similar between the two stimulation conditions (**Supplementary Fig. 7c–g**). As controls, we confirmed that magnetic stimulation initiated APs at a comparable rate to current injection (**Supplementary Fig. 8a**) and did not cause electrical interference in electrophysiology measurements (**Supplementary Fig. 8b**).

To test whether the magnetically evoked firing was due specifically to activation of TRPV4, we bathed brain slices in the selective TRPV4 antagonist GSK205 (*n* = 3 neurons from 3 mice). After a 10-min incubation with GSK205, magnetic stimulation failed to evoke APs (**Fig. 2c**), suggesting that the observed APs were due to Magneto2.0 activation. To determine whether magnetic stimulation affects mEC neurons not expressing Magneto2.0, we magnetically stimulated cells transduced with AAVs delivering *CMV::DIO-Magneto2.0* and *Camk2a::EGFP*, which does not induce Cre-dependent expression

of Magneto2.0. We found that stimulation with magnetic fields did not evoke APs in non-Magneto2.0-expressing EGFP⁺ neurons of the mEC, although these neurons fired spike trains in response to injection with 300 pA of depolarizing current (*n* = 6 neurons from 3 mice; **Fig. 2d** and **Supplementary Fig. 7h**). In sum, we found that only Magneto2.0-expressing neurons of the mEC fired APs in response to magnetic field stimulation, and bath application of GSK205 blocked these responses (**Fig. 2e**). These data support the notion that activation of Magneto2.0 can rapidly and reversibly depolarize neurons, leading to remote control over neural circuit dynamics.

Magnetic control over zebrafish tactile behaviors

We next began validation of Magneto2.0 function *in vivo*. We first sought to remotely modulate a simple behavior of the zebrafish, *Danio rerio*. We transiently expressed Magneto2.0 in Rohon-Beard sensory neurons (approximately 5 Magneto2.0⁺ Rohon-Beard neurons per fish, *n* = 9 fish), using regulatory sequences of the *neurog1* promoter[24,25]. We identified mosaic zebrafish expressing Magneto2.0 in Rohon-Beard neurons by selecting animals that also expressed a co-injected fluorescent marker in the heart (**Supplementary Fig. 9a**). We sought to determine whether magnetic stimulation of zebrafish expressing

Figure 3 Magnetic control over zebrafish tactile behavior *in vivo*. (**a**) Quantification of GCaMP3 fluorescence in mCherry⁺ Rohon-Beard sensory neurons and mCherry⁻ spinal cord neurons in 48 hpf zebrafish larvae expressing *neurog1::Magneto2.0-p2a-mCherry*. *n* = 20 mCherry⁺, *n* = 33 mCherry⁻ neurons from 8 stimulation experiments using *n* = 5 zebrafish from 2 independent injection cohorts. Two-way ANOVA, Bonferroni post-test, ($F_{42,2339}$ = 3.248, P < 0.0001). *P < 0.05 for all points from 35 to 55 s. (**b**) Coiling rate of 24–36 hpf *neurog1::Magneto2.0* fish. Number of independent experiments for each condition is *n* = 3 (no magnet) and *n* = 6 (magnet). *n* = 26 (no magnet) and *n* = 25 (magnet) fish were used in respective conditions. Unpaired two-tailed *t*-test, (t_7 = 6.152, P = 0.0005). (**c**) Fold change in coiling of fish genotypes aged 24–36 hpf. Number of videos analyzing baseline coiling is *n* = 3 per genotype, number of magnetic stimulation experiments include *n* = 4 (Uninjected), *n* = 4 (*neurog1::Trpv4-p2A-ferritin*) and *n* = 6 (*neurog1::Magneto2.0*). Number of fish analyzed shown as (baseline, magnet) for each genotype: uninjected (27, 18), *neurog1::Trpv4-p2A-ferritin* (17, 21) and *neurog1::Magneto2.0* (26, 25). One-way ANOVA, Bonferroni post-test ($F_{2,11}$ = 39.01, P < 0.0001). Data pooled from 2 independent injection cohorts per genotype. ***P < 0.001, *P < 0.05. Data shown as mean ± s.e.m.
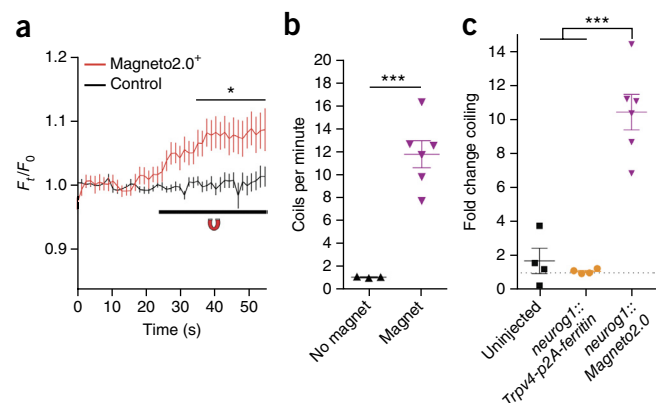
Figure 4 Magnetogenetic control of the mammalian nervous system *in vivo*. (**a**) Representation of magnetic stimulation and recording of D1R-expressing cells in the striatum (St) of *Drd1a::Cre* mice. Solid lines indicate electrode placement from 5 mice; dashed circle indicates approximate injection area. (**b**) Cartoon of magnetized testing chamber. Rare earth magnets (gray bars) are embedded in the walls; **B** represents magnetic field; magnetic field strength is shown as a gradient. (**c**) Quantification of single-unit average firing rate during magnetic field exposure in freely behaving mice. $n = 51$ <5-Hz neurons, $n = 81$ >5-Hz neurons from 5 mice ($n = 66$, $n = 30$, $n = 25$, $n = 7$, $n = 4$ cells, respectively). Unpaired two-tailed *t*-test, ($t_{130} = 3.210$, $P = 0.0017$). (**d**) Proportion of cells firing >5% over baseline during magnet exposure. (**e**) Standard score (*z*-score) over time for <5-Hz MSNs in **d** that fired >5% (red, $n = 23$) versus <5% (black, $n = 28$). Two-way ANOVA ($F_{1,5880} = 210.9$, $P < 0.0001$). Gray box represents stimulation in magnetized chamber. Dashed line shows baseline of no change. (**f**) Proportion of cells firing >5% over baseline after cessation of magnet exposure. Data are shown as mean ± s.e.m. ***$P < 0.001$, **$P < 0.01$.
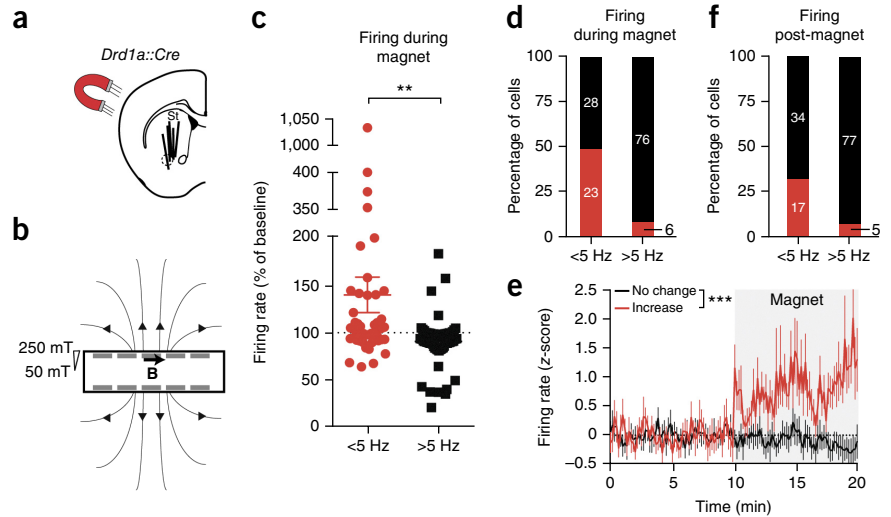
Magneto2.0 led to an increase in calcium signaling within Rohon-Beard neurons. To this end, we performed GCaMP imaging of live, 48 hours post-fertilization (hpf) zebrafish larvae expressing *Tg(s1020t::Gal4);Tg(UAS::GCaMP3);neurog1::Magneto2.0-p2a-mCherry*, which enables detection of activated neurons through the genetically encoded calcium sensor GCaMP3 (ref. 26), which is expressed in ventral spinal cord neurons[27]. This transgenic combination enables direct visualization of calcium transients in response to magnetic stimulation through dual labeling of GCaMP3^{+} and mCherry[+] Rohon-Beard neurons. We delivered a 50-mT static magnetic field via NdFeB rare earth magnets and observed an immediate increase in GCaMP3 fluorescence in stimulated Magneto2.0[+], mCherry-labeled Rohon-Beard neurons but not in adjacent mCherry^{−} neurons populating the spinal cord (**Fig. 3a** and **Supplementary Fig. 10a**). Seventeen of 20 mCherry^{+} neurons responded above the 6.9 ± 0.15% (mean ± s.e.m.) average maximal fluorescence change of control mCherry^{−} cells (**Supplementary Fig. 10a**), suggesting that magnetic stimulation *in vivo* will reliably activate Magneto2.0^{+} neurons, consistent with both our calcium imaging and slice electrophysiology data.

We next tested whether remote activation of Rohon-Beard neurons is sufficient to modulate the behavior of *neurog1::Magneto2.0* zebrafish in the presence or absence of magnetic fields. We developed a magnetized behavioral testing arena formed by spacing two NdFeB rare earth magnets 6 mm apart (**Supplementary Fig. 10b**), which delivered a tenfold greater magnetic field of ~500 mT to zebrafish larvae than the GCaMP assay. We hypothesized that even if only a few Rohon-Beard neurons were activated by Magneto2.0, the stereotypical escape response would nevertheless induce a coiling behavior, as demonstrated previously[25,28]. In response to a 500-mT magnetic field, groups of 24 to 34 h post fertilization (hpf) *neurog1::Magneto2.0*-expressing zebrafish larvae indeed coiled more frequently compared to those not exposed to a field (**Fig. 3b** and **Supplementary Movies 1** and **2**). In contrast to *neurog1::Magneto2.0* fish, which displayed an approximate tenfold increase in coiling behavior upon magnetic field exposure, there was no observable change in this behavior for either control group—uninjected wild-type fish or *neurog1::Trpv4-p2A-ferritin* fish, which bicistronically express independent, unfused TRPV4 and ferritin moieties (**Fig. 3c**). Consistent with *in vitro* findings, fish expressing the Magneto prototype channel under control of the

β-actin (*Actb1*) promoter exhibited a response that was one-fifth that of fish expressing Magneto 2.0 (**Supplementary Fig. 9b–d**). Finally, we confirmed that Magneto2.0 expression did not disrupt normal peripheral projections of Rohon-Beard neurons by examining red fluorescent protein (RFP) expression in sensory neurons of *Tg(isl1::rfp)* fish and *Tg(isl1::rfp);neurog1::Magneto2.0-IRES-nlsegfp* chimeric fish (**Supplementary Fig. 10c–f**). Together, these results confirm that Magneto2.0 is a viable candidate for remotely controlling neuronal activity and animal behavior *in vivo*.

## Remote control of neural activity in freely behaving mice

To determine whether Magneto2.0 is capable of controlling mammalian neural activity *in vivo*, we performed electrophysiology measurements in freely behaving mice transduced with an AAV1 carrying *CMV::DIO-Magneto2.0*, which expresses Magneto2.0 in a Cre-dependent manner. We aimed to test whether Magneto2.0 is capable of rapidly activating a large nucleus deep within the brain, which is more challenging when using optical actuators. To this end, we used mice expressing Cre recombinase under control of the dopamine receptor 1 promoter (*Drd1a::Cre*), which is expressed in approximately half the medium spiny neurons (MSNs) of the striatum[29]. We then transduced striatal neurons of *Drd1a::Cre* mice with an AAV1 carrying Magneto2.0 and, 3 weeks after viral injection, performed extracellular single-unit recordings with tetrode microdrives on Magneto2.0-expressing striatal cells in freely behaving mice and examined the effects of magnetic stimulation on neural firing (**Fig. 4a**). For this assay, we designed a magnetized chamber (23 cm × 4 cm × 18 cm) consisting of NdFeB magnets embedded in the chamber walls (**Fig. 4b**) and quantified the firing rates of striatal neurons under three conditions: at baseline without magnetic stimulation, during exposure to 50–250 mT magnetic fields in the chamber, and after magnetic field exposure. We classified recorded cells into two main groups based on firing rate: slow-spiking (<5 Hz) and fast-spiking (>5 Hz) neurons with mean firing rates of 2.1 ± 0.3 Hz (mean ± s.e.m.) and 8.6 ± 0.6 Hz (mean ± s.e.m.), previously described as putative MSNs (either D1R[+]D2R[−] or D1R[−]D2R[+]) and GABAergic interneurons (D1R[−]), respectively[30]. Exposure of these mice to magnetic fields produced a 43.8 ± 20.3% increase in the overall firing rate of slow-spiking putative MSNs (**Fig. 4c–e**). The firing rate of putative GABAergic interneurons

Figure 5 Activation of striatal D1R+ neurons is sufficient to control reward behavior. (**a**) Cartoon of magnetized RTPP assay. (**b**–**d**) Representative heat maps of arm preference for each condition shown as time spent in a particular arm; midpoint of one mouse shown per map. Heat map scale shown as relative time spent in a given location. WT, wild type. (**e**) Difference in time spent in magnetic arm versus non-magnetic arm for WT and *Drd1a::Cre* mice (*n* = 6 per genotype) transduced with an AAV1 carrying *CMV::DIO-Magneto2.0* during a ten-minute testing session. "No magnet" refers to unmagnetized RTPP chamber, "magnet" refers to magnetized chamber. WT mice were tested in the magnetized chamber only. One-way ANOVA, Bonferroni post-test ($F_{2,15}$ = 5.611, P = 0.0152). Data are shown as mean ± s.e.m. *$P < 0.05$.

remained constant (**Fig. 4c,d**). After cessation of magnetic stimulation, 66.7% of putative MSNs returned to baseline firing rates, while the putative interneuron firing rate again remained at baseline (**Fig. 4f**). Finally, we observed an increase in the firing rate of slow-spiking, but not fast-spiking, neurons of the striatum following systemic administration of the D1R agonist SKF81297 (**Supplementary Fig. 11a**), suggesting that the D1R+ population responsive to magnetic fields are indeed slow-spiking neurons. Together, these data demonstrate that Magneto2.0 is capable of controlling neural firing in deep brain regions in response to magnetic fields.

Control of D1R-mediated striatal reward valence

Ultimately, we sought to determine whether Magneto2.0 dependent control of neural activity *in vivo* could translate to control over complex mammalian reward behaviors regulated by dopamine signaling[31]. While optogenetic studies have implicated the dopaminergic signaling axis in reward behavior[32], it is unclear whether activation of postsynaptic D1R+ neurons is sufficient for controlling this effect. For instance, optogenetic stimulation of one subset of striatal D1R+ neurons is not sufficient to induce conditioned place preference[33]. Conversely, studies using systemic pharmacological manipulations with D1R agonists confirm that activation of D1R+ neurons is sufficient to evoke conditioned place preference[34,35], suggesting that broadly activating D1R+ neurons may cause reinforcing behaviors. Optogenetic techniques are intrinsically limited in the number of neurons that can be activated simultaneously via fiber optic implants and pharmacological approaches lack genetic specificity. However, a magnetogenetic approach circumvents both obstacles, allowing resolution of this discrepancy with cell-type specificity and a real-time behavioral output. We tested the sufficiency of D1R+ neurons in eliciting reward conditioning by unilaterally injecting the striata of wild-type and *Drd1a::Cre* mice with an AAV1 carrying *CMV::DIO-Magneto2.0* and subjecting the mice to a real-time place preference (RTPP) assay where they could choose between a magnetized arm, lined with eight permanent NdFeB magnets delivering a magnetic field gradient of 250–50 mT, and an unmagnetized arm (**Fig. 5a**). Magneto2.0-expressing *Drd1a::Cre* mice showed a significant preference for the magnetized arm of the RTPP chamber, in contrast to wild-type mice (one-way ANOVA, P = 0.0152), which exhibited no preference (**Fig. 5b–e**). Moreover, removal of the magnets from the chamber eliminated the preference of Magneto2.0-expressing *Drd1a::Cre* mice for either arm, yielding a response identical to wild-type mice (**Fig. 5c**). Thus, RTPP is dependent on D1R+ neuron stimulation. As a control, we measured no differences in overall locomotion between unilaterally injected wild-type and *Drd1a::Cre* mice using a modified open field assay (**Supplementary Fig. 11b,c**). These data show, first, that broad activation of D1R+ neurons of the striatum is sufficient to control reward salience and, second, that Magneto2.0 can be used for remote control of complex mammalian behaviors mediated by deep brain nuclei in freely moving mice.
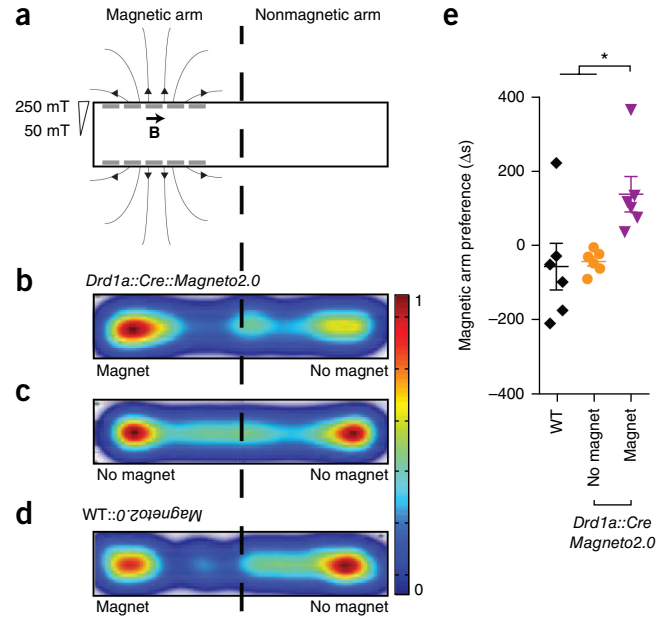
DISCUSSION

In total, we have engineered and optimized a genetically encoded magnetogenetic actuator, Magneto2.0, and applied it to the nervous system in freely behaving animals. This is, to our knowledge, the first demonstration of bona fide magnetic control of the nervous system using engineered actuators, which we confirmed electrophysiologically and behaviorally using both zebrafish and mice. We have shown that Magneto2.0 remotely controlled both neural firing rates and behavior on a rapid and physiologically relevant timescale, which is a prediction offered by the authors of an earlier study employing magnetogenetics to study insulin signaling[11]. Our single-component magnetogenetic system represents an advance in the ability to study neural circuits with relative ease, as broad populations of genetically defined cells can be remotely activated in freely behaving animals. We applied Magneto2.0 to the study of reward behaviors to directly measure the behavioral consequences involved in remotely modulating large populations of cells participating in specific neural circuits[36]. Our findings also shed light on the sufficiency of D1R+ neurons to control reinforcing behaviors, which is consistent with the results of a recent study investigating D1R+ neuron necessity in these processes[37].

Magneto2.0 represents a prototype for a class of magnetogenetic remote controlled actuators. While we initiated our actuator design using TRPV4 because of its small size and known pressure sensitivity[13,38–40], Magneto suffers from the unique disadvantage of remaining sensitive to several endogenous stimuli known to activate TRPV4 (refs. 14,15), a problem not encountered with many opto- or chemogenetic methods. Future studies may be able to optimize Magneto2.0 such that it no longer responds to these stimuli and responds to magnetic fields only. In addition, it will be useful to understand whether Magneto functions because of the mechanosensitive nature of TRPV4 or whether this property is immaterial to its magnetic activation. Continued optimization and utilization of this magnetogenetic actuator will position the field to better understand neural development, function and pathology.

METHODS

Methods and any associated references are available in the online version of the paper.

TECHNICAL REPORTS

AUTHOR CONTRIBUTIONS
M.A.W. and A.D.G. designed the study. M.A.W., C.J.S., M.O., B.S.B., A.M.P., R.M.G., R.P.G., A.J.S. and M.P.B. performed the experiments. M.A.W., C.J.S., M.O., B.S.B., A.M.P., R.M.G., M.K.P., C.D.D. and A.D.G. analyzed the data. S.K., M.K.P., C.D.D. and A.D.G. supervised the research. M.A.W. and A.D.G. wrote the manuscript with input from coauthors.

1. Zemelman, B.V., Lee, G.A., Ng, M. & Miesenböck, G. Selective photostimulation of genetically chARGed neurons. *Neuron* **33**, 15–22 (2002).
2. Boyden, E.S., Zhang, F., Bamberg, E., Nagel, G. & Deisseroth, K. Millisecond-timescale, genetically targeted optical control of neural activity. *Nat. Neurosci.* **8**, 1263–1268 (2005).
3. Gradinaru, V., Mogri, M., Thompson, K.R., Henderson, J.M. & Deisseroth, K. Optical deconstruction of parkinsonian neural circuitry. *Science* **324**, 354–359 (2009).
4. Sternson, S.M. & Roth, B.L. Chemogenetic tools to interrogate brain functions. *Annu. Rev. Neurosci.* **37**, 387–407 (2014).
5. Alexander, G.M. *et al.* Remote control of neuronal activity in transgenic mice expressing evolved G protein-coupled receptors. *Neuron* **63**, 27–39 (2009).
6. Güler, A.D. *et al.* Transient activation of specific neurons in mice by selective expression of the capsaicin receptor. *Nat. Commun.* **3**, 746 (2012).
7. Bernstein, J.G., Garrity, P.A. & Boyden, E.S. Optogenetics and thermogenetics: technologies for controlling the activity of targeted cells within intact neural circuits. *Curr. Opin. Neurobiol.* **22**, 61–71 (2012).
8. Hughes, S., McBain, S., Dobson, J. & El Haj, A.J. Selective activation of mechanosensitive ion channels using magnetic particles. *J. R. Soc. Interface* **5**, 855–863 (2008).
9. Huang, H., Delikanli, S., Zeng, H., Ferkey, D.M. & Pralle, A. Remote control of ion channels and neurons through magnetic-field heating of nanoparticles. *Nat. Nanotechnol.* **5**, 602–606 (2010).
10. Stanley, S.A. *et al.* Radio-wave heating of iron oxide nanoparticles can regulate plasma glucose in mice. *Science* **336**, 604–608 (2012).
11. Stanley, S.A., Sauer, J., Kane, R.S., Dordick, J.S. & Friedman, J.M. Remote regulation of glucose homeostasis in mice using genetically encoded nanoparticles. *Nat. Med.* **21**, 92–98 (2015).
12. Chen, R., Romero, G., Christiansen, M.G., Mohr, A. & Anikeeva, P. Wireless magnetothermal deep brain stimulation. *Science* **347**, 1477–1480 (2015).
13. Loukin, S., Zhou, X., Su, Z., Saimi, Y. & Kunsg, C. Wild-type and brachyolmia-causing mutant TRPV4 channels respond directly to stretch force. *J. Biol. Chem.* **285**, 27176–27181 (2010).
14. Liedtke, W. *et al.* Vanilloid receptor-related osmotically activated channel (VR-OAC), a candidate vertebrate osmoreceptor. *Cell* **103**, 525–535 (2000).
15. Güler, A.D. *et al.* Heat-evoked activation of the ion channel, TRPV4. *J. Neurosci.* **22**, 6408–6414 (2002).
16. Stanley, S. Biological nanoparticles and their influence on organisms. *Curr. Opin. Biotechnol.* **28**, 69–74 (2014).
17. Iordanova, B., Robison, C.S. & Ahrens, E.T. Design and characterization of a chimeric ferritin with enhanced iron loading and transverse NMR relaxation rate. *J. Biol. Inorg. Chem.* **15**, 957–965 (2010).
18. Lei, L. *et al.* A TRPV4 channel C-terminal folding recognition domain critical for trafficking and function. *J. Biol. Chem.* **288**, 10427–10439 (2013).
19. Hofherr, A., Fakler, B. & Klöcker, N. Selective Golgi export of Kir2.1 controls the stoichiometry of functional Kir2.x channel heteromers. *J. Cell Sci.* **118**, 1935–1943 (2005).
20. Gradinaru, V. *et al.* Molecular and cellular approaches for diversifying and extending optogenetics. *Cell* **141**, 154–165 (2010).
21. Lytton, J., Westlin, M. & Hanley, M.R. Thapsigargin inhibits the sarcoplasmic or endoplasmic reticulum Ca-ATPase family of calcium pumps. *J. Biol. Chem.* **266**, 17067–17071 (1991).
22. Phan, M.N. *et al.* Functional characterization of TRPV4 as an osmotically sensitive ion channel in porcine articular chondrocytes. *Arthritis Rheum.* **60**, 3028–3037 (2009).
23. Sohal, V.S., Zhang, F., Yizhar, O. & Deisseroth, K. Parvalbumin neurons and gamma rhythms enhance cortical circuit performance. *Nature* **459**, 698–702 (2009).
24. Andermann, P., Ungos, J. & Raible, D.W. Neurogenin1 defines zebrafish cranial sensory ganglia precursors. *Dev. Biol.* **251**, 45–58 (2002).
25. Douglass, A.D., Kraves, S., Deisseroth, K., Schier, A.F. & Engert, F. Escape behavior elicited by single, channelrhodopsin-2-evoked spikes in zebrafish somatosensory neurons. *Curr. Biol.* **18**, 1133–1137 (2008).
26. Tian, L. *et al.* Imaging neural activity in worms, flies and mice with improved GCaMP calcium indicators. *Nat. Methods* **6**, 875–881 (2009).
27. Wyart, C. *et al.* Optogenetic dissection of a behavioural module in the vertebrate spinal cord. *Nature* **461**, 407–410 (2009).
28. Sagasti, A., Guido, M.R., Raible, D.W. & Schier, A.F. Repulsive interactions shape the morphologies and functional arrangement of zebrafish peripheral sensory arbors. *Curr. Biol.* **15**, 804–814 (2005).
29. Hersch, S.M. *et al.* Electron microscopic analysis of D1 and D2 dopamine receptor proteins in the dorsal striatum and their synaptic relationships with motor corticostriatal afferents. *J. Neurosci.* **15**, 5222–5237 (1995).
30. Berke, J.D., Okatan, M., Skurski, J. & Eichenbaum, H.B. Oscillatory entrainment of striatal neurons in freely moving rats. *Neuron* **43**, 883–896 (2004).
31. Wise, R.A. Dopamine, learning and motivation. *Nat. Rev. Neurosci.* **5**, 483–494 (2004).
32. Tsai, H.-C. *et al.* Phasic firing in dopaminergic neurons is sufficient for behavioral conditioning. *Science* **324**, 1080–1084 (2009).
33. Lobo, M.K. *et al.* Cell type-specific loss of BDNF signaling mimics optogenetic control of cocaine reward. *Science* **330**, 385–390 (2010).
34. Zengin-Toktas, Y. *et al.* Motivational properties of D2 and D3 dopamine receptors agonists and cocaine, but not with D1 dopamine receptors agonist and L-dopa, in bilateral 6-OHDA-lesioned rat. *Neuropharmacology* **70**, 74–82 (2013).
35. Gore, B.B. & Zweifel, L.S. Genetic reconstruction of dopamine D1 receptor signaling in the nucleus accumbens facilitates natural and drug reward responses. *J. Neurosci.* **33**, 8640–8649 (2013).
36. Stuber, G.D., Britt, J.P. & Bonci, A. Optogenetic modulation of neural circuits that underlie reward seeking. *Biol. Psychiatry* **71**, 1061–1067 (2012).
37. Jeong, J.W. *et al.* Wireless optofluidic systems for programmable *in vivo* pharmacology and optogenetics. *Cell* **162**, 662–674 (2015).
38. O'Neil, R.G. & Heller, S. The mechanosensitive nature of TRPV channels. *Pflugers Arch.* **451**, 193–203 (2005).
39. Liedtke, W. & Kim, C. Functionality of the TRPV subfamily of TRP ion channels: add mechano-TRP and osmo-TRP to the lexicon! *Cell. Mol. Life Sci.* **62**, 2985–3001 (2005).
40. Matthews, B.D. *et al.* Ultra-rapid activation of TRPV4 ion channels by mechanical forces applied to cell surface beta1 integrins. *Integr. Biol. (Camb.)* **2**, 435–442 (2010).

ONLINE METHODS

Mouse information. All animal experiments were conducted in accordance with the University of Virginia Institutional Animal Care and Use Committee (IACUC). All mice were maintained on a C57Bl/6 background. Mice were housed in a vivarium on a 12-h light/dark cycle at one to three mice per cage. Viral injection experiments were conducted starting at 8 weeks of age. All mice used in this study were injected between 8 and 10 weeks of age. Only male mice were used in this study.

Zebrafish husbandry. All animal studies were approved by the University of Virginia IACUC. Zebrafish strains used in this study were as follows: AB*, *Tg(isl1::rfp)* and *Tg(s1020t::Gal4);Tg(UAS::GCaMP3)*. Embryos were raised at 28.5 °C in egg water or embryo medium and staged according to hours post-fertilization (hpf) or days post-fertilization (dpf). Embryos of both sexes were used for experiments[41].

Molecular biology. Molecular biology was performed using standard protocols. Plasmid DNA was purified using kits from Qiagen. Restriction enzymes were purchased from New England Biolabs. Amplification of template DNA was performed with Phusion Flash (Life Technologies, F-548) and sequenced by GeneWiz. For TRPV4 S4-S5 fusion proteins, site-directed mutagenesis using QuikChange II XL (Agilent) was performed on TRPV4 to introduce a unique BamHI site, into which a successive series of DNA linkers is inserted to gradually expand the linker region flanking TRPV4 and ferritin.

Rat *Trpv4* was obtained from Addgene vector 45751, a gift from R. Lefkowitz. To generate AAV expression vectors, we modified Addgene vector 35507, a gift from K. Deisseroth. A *CMV* promoter was substituted in the 35507 vector and a short poly(A) sequence was used[42] to minimize size of the vector. A human ferritin L-H fusion gene was designed according to a previous study[17] and synthesized by IDT. Other than AAV vectors, mammalian expression vectors were maintained in the pcDNA3.0 backbone. Fish expression vectors were maintained in pDestTol2CG2, and all entry vector maps are freely available from http://tol2kit.genetics.utah.edu/. Relevant plasmids used in this study will be deposited in Addgene.

Magnets and magnetic field strength measurement. Electromagnets of varying sizes and strengths were purchased from eBay (seller ID: pawnnew). Permanent N42- or N52-grade NdFeB magnets were purchased from CMS Magnetics. Gaussmeters (AlphaLabs, Inc.) were used to determine the field strength of electromagnets over distance for each experiment. For the *in vivo* zebrafish and mouse behavioral experiments using permanent NdFeB magnets, an online magnetic field calculator (K&J Magnetics) or a gaussmeter (AlphaLabs, Inc.) was used.

Cell transfection and cell culture. HEK293 cells were a gift from the University of Virginia tissue culture core. Cells used in this study were authenticated and checked for mycoplasma contamination. Cells were transfected using Lipofectamine 2000 (Invitrogen) according to standard protocols. Low passage (<40) HEK293 cells were transfected for 1–2 h in well plates, trypsinized for 5 min using 0.25% trypsin (wt/vol), and replated onto glass coverslips coated with poly-D-lysine (50 µg/mL) and laminin (1 µg/mL) in fresh DMEM:F12 medium (Life Technologies) containing 1 mM nonessential amino acids (Gibco), 1 mM sodium pyruvate (Gibco), 10% FBS and 1× penicillin/streptomycin (Gibco).

Microscopy. Imaging for calcium imaging and immunocytochemistry was performed on a Leica SP5 confocal with white light laser. Calcium imaging was performed using 10× magnification.

***In vitro* magnetic calcium imaging.** Calcium imaging was performed largely as described previously[15,43]. Briefly, transfected cells were plated on glass coverslips and incubated overnight in a humidified incubator kept at 37 °C and 10% CO_2. Cells were washed three times with calcium imaging buffer (CIB) (105 mM NaCl, 3 mM KCl, 2.5 mM $CaCl_2$, 0.6 mM $MgCl_2$, 10 mM HEPES, 1.2 mM $NaHCO_3$, 100 mM mannitol and 10 mM glucose, adjusted to pH 7.45 with NaOH) and loaded with 3 µM Fluo-4 diluted in CIB for 30 min at 37 °C. Cells were then washed three times with CIB and de-esterified for 30–60 min at 37 °C. Coverslips were then loaded into customized imaging chambers and imaged at 10× magnification

for analysis. Ruthenium red (RR), a TRP channel pore blocker (Sigma), was used at a concentration of 10 µM and cells were incubated with RR for ~2–3 min in the imaging chambers before imaging. For calcium-free medium experiments, calcium in CIB was replaced with 10 mM EGTA and cells were washed and incubated with calcium-free medium. The TRPV4 specific antagonist GSK205 was purchased from Calbiochem (616522) and used at a concentration of 10 µM. Cells were incubated in GSK205 for 15 min at 37 °C before calcium imaging.

A magnetic stimulus was delivered using 3-cm electromagnets (purchased from eBay, seller ID: pawnnew) rated for continuous duty, 12 V DC, 5 W and 10 kg of pull force. We situated the magnet directly above the imaging chamber during imaging. Using a gaussmeter (AlphaLab Inc.), we calculated the magnetic field experienced by the cells (~1.25 cm away from the magnet) to be roughly 40–50 mT (**Supplementary Fig. 1**). Imaging was performed by recording 30 s of baseline fluorescence and then turning on the magnet for 3–6 pulses of 10 s each (0.1 Hz, total time of 30–60 s, 90% duty cycle), using a standard DC power delivery system. Coverslips were not analyzed if they shifted noticeably during imaging.

Cells were randomly selected from an image field. Quantification was performed by averaging 30 s of baseline fluorescence measurements with no applied magnetic field followed by quantification of the largest three fluorescence values following magnetic stimulation. The three peak values were normalized to the average baseline fluorescence before magnetic stimulation to compute a relative fold change for each cell. Fold change was normalized to background by respectively scaling all values by the average fold change in the background (if applicable) during magnetic stimulation. For time course analyses (**Fig. 1g,h**), fluorescence data for each cell were analyzed as a relative increase over time compared to the baseline fluorescence (30 s) before magnetic stimulation.

Thapsigargin calcium imaging. HEK cells were prepared for calcium imaging as above. Thapsigargin was purchased from Sigma (T9033) and used at a working concentration of 1 µM, diluted 1:1,000 in CIB. A 30-s baseline of calcium fluorescence was recorded before direct application of 800 µL of thapsigargin to the calcium imaging chamber. Calcium fluorescence was recorded for 1 h after thapsigargin addition (**Supplementary Fig. 6a**).

Magneto2.0-expressing cells were treated with thapsigargin and incubated at 37 °C for 30 min before calcium imaging, as thapsigargin-induced calcium release remained steady at 30 min after application. Cells were stimulated with magnetic fields as above: 10-s pulses of 50-mT field for 30 s of total field exposure.

Immunocytochemistry. Cells plated on coverslips were washed three times with PBS, fixed in 4% PFA for 1 h at room temperature, washed three times with PBS and mounted on slides with Fluoromount-G with DAPI (Southern BioTech). Immunocytochemistry for each iteration of trafficking signals was performed on two independent populations of transfected HEK293 cells.

Fish injection. AB* or *Tg(isl1::rfp)* embryos were injected at the one-cell stage with 1–2 nL of a working stock of 12.5 ng/µL DNA for each construct. At 24 hpf, embryos were screened for *cmcl2::egfp*⁺ transgenics. Imaging of *cmcl2::egfp* expression was performed on every zebrafish embryo examined (*n* > 50 positive fish).

Zebrafish GCaMP3 live imaging. Zebrafish expressing *Tg(s1020t::Gal4);Tg(UAS::GCaMP3);neurog1::Magneto2.0-p2A-mCherry* were mounted in 0.8–2% low melting point agarose and imaged on a Leica SP5 laser-scanning confocal microscope with a white light laser. Fish were imaged using a 40× objective with water immersion. After 30–60 s of baseline fluorescence readings, mounted zebrafish were stimulated by a ~50-mT magnetic field delivered by a permanent NdFeB rare earth magnet. The confocal pinhole was increased to 2 µm and the scan speed was approximately 1.3 s per frame. *n* = 5 fish and *n* = 8 stimulation experiments were analyzed from two independent pools of injections.

***In vivo* zebrafish imaging.** Imaging was performed as described previously[44]. Briefly, we used a Quorum WaveFX-XI spinning disc confocal system (Quorum Technologies Inc.) equipped with a 40× water objective (NA = 1.1) on a motorized Zeiss AxioObserver ZI microscope. Images were processed with Metamorph. *n* = 10 fish imaged per genotype.

Zebrafish behavioral tests. Injected fish were maintained on an AB* background strain. Zebrafish embryos were behaviorally tested 24–34 hpf. Two 2 × 0.5 × 0.25 inch

N52-grade NdFeB permanent magnets were oriented such that one south and one north pole were oriented toward the fish over a fixed distance of ~1 cm. Fish were maintained in egg water during the course of behavioral testing and a 30-fps video was taken using an Axio Zoom.V16 fluorescence stereo zoom microscope. Fish were randomly selected from their groups for behavioral analysis. The videos were manually scored by counting the number of coils made by each fish over the length of the video and normalized to give a rate of coiling by dividing the number of coils by the length of the video. Length of original behavioral analysis was 2–3 min per video and **Supplementary Movies 1** and **2** are shown at 8× speed. Fish tested had no prior history of behavioral testing. Animals were tested once each. Exclusion criteria for analysis consisted of stereotypy such as continuous coiling during the recording of the movie. Two uninjected wild-type animals were excluded from the analysis given these criteria. Behavioral testing was performed during the day at consistent times (8 am–4 pm).

Zebrafish whole mount immunostaining. Zebrafish were fixed and immunostained according to the protocol described previously[44]. The antibody used was rabbit anti-GFP (Invitrogen, A-6455) at a dilution of 1:1,000. The secondary antibody was donkey anti-rabbit Alexa 488 (Invitrogen, A-21206) used at 1:600.

Stereotaxic injection. *Striatum transduction:* The AAV1 *CMV::DIO-Magneto2.0-pA* virus used in this study was produced in the University of Pennsylvania vector core. Four injections of 1 μL of AAV1 virus with a titer of ~5 × 10^{12} were injected unilaterally into the striata of wild-type and *D1R::Cre* mice using a 30G Hamilton syringe, stereotaxic alignment system (Cartesian Research, Inc.) and automated delivery system (World Precision Instruments) while mice were under 2% isoflurane anesthesia on a heating pad. Unilateral injection was performed at (M/L: +1.6, A/P: +0.98) relative to bregma and four 1-μL injections were performed at depths of −4.75, −3.75, −2.75 and −1.75 mm over 40 min at a rate of 100 nL/min. After the final injection, the syringe was kept in the brain for 10 min, raised 0.5 mm where it remained for 5 min, then removed. Mice were administered 3 mg/kg ketoprofen after injection and for 3 subsequent days and permitted to recover on a heating pad before being returned to their home cages.

mEC transduction. For expression of Magneto 2.0 in hippocampal and mEC neurons, C57Bl/6 mice (5–6 weeks old) were anesthetized with ketamine/dexmedetomidine solution and mounted on a stereotaxic apparatus. Anesthesia was maintained by inhaled isoflurane for the duration of the procedure. A small hole was opened in the skull and a pulled glass micropipette was lowered to the target site (M/L: ±3.0, A/P: −3.0) at a depth of 2.0 mm. Mice were injected with an equivolume mixture of an AAV1 carrying *CMV::DIO-Magneto2.0* and an AAV9 carrying *Camk2a::EGFP-Cre* (obtained from UPenn Vector Core) with titers of ~5 × 10^{12} and ~1 × 10^{13} infectious units per mL, respectively. Virus (200 nL) was injected with pressure at a rate of ~50 nL/min. After injection the micropipette was maintained in place for 4 min before retraction. This procedure was repeated bilaterally. Mice were allowed to recover for at least 4 weeks after surgery before electrophysiology testing.

Brain slice electrophysiology. Horizontal brain slices were prepared as previously described[45]. For recordings, slices were held in a small chamber superfused with heated (32 °C) oxygenated ACSF at 3 mL/min. For electrophysiology experiments, transduced mouse medial entorhinal cortex neurons were visually identified by EGFP fluorescence using a Zeiss Axioscope microscope (Zeiss, Oberkochen, Germany). Action potentials were evoked using a current injection step to 300 pA. To evoke action potentials via magnetic stimulus, a permanent NdFeB magnet (CMS Magnetics) was used delivering ~50 mT. The magnet was driven toward the EGFP+ neuron via a micromanipulator until it was approximately 1 cm from the cell. Action potential parameters were measured as previously described[45].

Single-unit recordings *in vivo* in freely moving mice. *In vivo* electrophysiology was performed largely as described previously[6]. HS-16 four-tetrode microdrives (Neuralynx) were implanted in anesthetized mice by using stereotaxic coordinates for the striatum described above, except that two injections of 1 μL each were made at depths of −4.75 mm and −4.25 mm in the brain; the headstage was installed at an initial depth of −4 mm. After 2 weeks of recovery, mice were connected to a digital Lynx (10S) acquisition system through an HS-16 headstage

preamplifier (Neuralynx), and signals were amplified and filtered (600–6,000 Hz). Data were acquired by using Cheetah acquisition software (Neuralynx). Baseline putative D1R neuron firing properties were recorded for 10 min in the unmagnetized arm of the custom-made place preference chamber, followed by 10 min in the magnetic arm of the chamber and then 10 min of a second baseline recording period. Tetrodes were lowered 50 μm daily during scanning for distinct units. Offline Sorter software (Plexon) cluster analysis was used to isolate units. Clustered waveforms were subsequently analyzed with MATLAB (MathWorks). Baseline activity recordings (10 min) were used to identify putative D1R neurons that exhibited firing rates below 5 Hz. Behavioral testing was performed at consistent times daily (9 am–1 pm) for 2–4 weeks. One mouse was excluded from this analysis because it did not yield at least four units.

After the completion of these three recording sessions, the mice were injected with the D1R agonist SKF81297 (Cayman Chemical, diluted to 3 mg/kg in saline, injected i.p.). Fifteen minutes after the agonist had been administered, a final 10-min recording period in the unmagnetized arm of the place preference chamber was completed. Drug injection experiments were performed only during a 5-d period following the triplicate recording procedure performed above (baseline, magnet, post-magnet). Data were not included in the triplicate analysis (**Fig. 4**) once a mouse had been injected with SKF81297. Data in **Supplementary Figure 11a** using drug are from a single mouse.

Immunohistochemistry. Mice were perfused with 4% PFA in PBS. Brains were removed and postfixed overnight at 4 °C, followed by dehydration in 30% sucrose for 2 d at 4 °C. Brains were frozen in OCT and sectioned on a cryostat into 30-μm sections. Tissue was washed three times as free-floating sections for 5 min with 0.3% PBS-T (Triton X-100), followed by blocking for 30 min in 5% donkey serum diluted in 0.3% PBS-T. Sections were then incubated with primary antibody diluted in blocking solution overnight at 4 °C with agitation. The next day, sections were washed three times for 5 min with 0.3% PBS-T, followed by incubation with secondary antibody diluted in blocking solution for 2 h at room temperature. Sections were washed three times for 5 min in 0.3% PBS-T and mounted on slides.

Primary antibodies used in this study were rabbit anti-TRPV4 (Santa Cruz, sc-98592) and rabbit anti-TRPV4 (Novus, NB110-74960). Secondary antibody used was donkey anti-rabbit Alexa-488 (Invitrogen A-21206) at 1:500.

The TRPV4 antibodies used showed high background staining in wild-type and untransduced tissue, making it difficult to distinguish between endogenous and virally mediated TRPV4 expression.

Mouse behavioral testing. All testing was conducted was during the mouse light cycle at consistent times (9 am–5 pm).

Open field. A custom-built open-field chamber was constructed by A.J.S. and M.A.W. (23 cm × 23 cm), with four 10-cm-diameter electromagnets fit into the floor and covered with a 0.5-cm wooden platform on which the mouse could walk. Each magnet was connected to an independent power supply delivering roughly 2.5 A and 30 V of power and generating a magnetic field of roughly 150 mT. Mice were placed in the chamber for 5 min and baseline recordings of locomotion were made. Magnets were turned on for 5 min to measure responses to the magnetic field. Each mouse was tested in the assay one time for a total of 10 min per mouse.

Real time place preference (RTPP). The two arms of the assay were custom-built by A.J.S. and M.A.W. (4 cm wide (internal diameter) × 23 cm long). Five permanent NdFeB magnets (four magnets 2 × 0.5 × 0.25 inches, one magnet 1 × 0.5 × 0.25 inches) were embedded into each wall of the magnetized arm, recessed at a depth of 1 cm. Each of the magnets delivered roughly 250 mT, and the magnetic field strength was roughly 50 mT in the center of the magnetized arm. The magnets were embedded at a height range of 1.1 to 1.6 cm above the floor of the chamber to primarily expose the heads of the mice to the field. Mice were placed into the chamber in the center of the two arms and permitted to explore for 2 min before recording began. The testing session lasted a total of 10 min. The two arms were constructed to appear identical except for the presence/absence of magnets.

For experiments using Magneto-transduced *Drd1a::Cre* mice in which the magnets were removed from the RTPP chamber, two cohorts of 3 mice each were used. In the first cohort, the mice were first exposed to the magnet on day 1, then the magnets were removed and preference was assessed on day 2.

In the second cohort, *Drd1a::Cre* mice injected with AAV1 *CMV::DIO-Magneto2.0* were trained in the chamber lacking magnets on day 1, then tested with the magnetized chamber on day 2. The magnetized and unmagnetized arms were transposed for each cohort to ensure that there was no preference for either side in the testing chamber.

Mouse behavioral data analysis. Mouse behaviors were measured using EthoVision XT 11 (Noldus), which is an automated tracking, recording and measurement software package. Following each testing session in the open field, linear velocity was measured (nose-point relative to center-point) with and without magnetic field for the open field assay. For RTPP, side preference was calculated as the percentage of time a mouse spent in the magnetized versus unmagnetized arm. For RTPP experiments in which mice were exposed to the chamber without any magnets installed, the 'magnetic arm' was chosen as the side where the magnet was placed in the testing session and numerical values were then calculated.

Statistical methods. All statistical comparisons were performed using Prism 6 (GraphPad). No omnibus normality test was performed for any of the data sets because sample sizes were small. Data were assumed to be normally distributed except in **Figure 4d,f** and **Supplementary Figure 9c**. Specific statistical tests are explicitly stated in the figure legends. No statistical methods were used to predetermine sample sizes, but our sample sizes are similar to those generally employed in the field[6,11,32,43,46,47]. No blinding was performed for data analysis or behavioral testing, but automated and randomized quantification was performed where applicable.

A **Supplementary Methods Checklist** is available.

41. Kimmel, C.B., Ballard, W.W., Kimmel, S.R., Ullmann, B. & Schilling, T.F. Stages of embryonic development of the zebrafish. *Dev. Dyn.* **203**, 253–310 (1995).
42. McFarland, T.J. *et al.* Evaluation of a novel short polyadenylation signal as an alternative to the SV40 polyadenylation signal. *Plasmid* **56**, 62–67 (2006).
43. Wheeler, M.A. *et al.* TNF-α/TNFR1 signaling is required for the development and function of primary nociceptors. *Neuron* **82**, 587–602 (2014).
44. Smith, C.J., Morris, A.D., Welsh, T.G. & Kucenas, S. Contact-mediated inhibition between oligodendrocyte progenitor cells and motor exit point glia establishes the spinal cord transition zone. *PLoS Biol.* **12**, e1001961 (2014).
45. Hargus, N.J., Nigam, A., Bertram, E.H. III & Patel, M.K. Evidence for a role of Nav1.6 in facilitating increases in neuronal hyperexcitability during epileptogenesis. *J. Neurophysiol.* **110**, 1144–1157 (2013).
46. Quintana, A. *et al.* Lack of GPR88 enhances medium spiny neuron activity and alters motor- and cue-dependent behaviors. *Nat. Neurosci.* **15**, 1547–1555 (2012).
47. Chen, S., Chiu, C.N., McArthur, K.L., Fetcho, J.R. & Prober, D. TRP channel mediated neuronal activation and ablation in freely behaving zebrafish. *Nat. Methods* **13**, 147–150 (2016).